IAC–19–C1.1.10

Low-Thrust Trajectory Design for a Cislunar CubeSat Leveraging Structures from the Bicircular Restricted Four-Body Problem

Robert Pritchett
Purdue University, USA, pritcher@purdue.edu

Kathleen C. Howell
Purdue University, USA, howell@purdue.edu

David C. Folta
NASA Goddard Space Flight Center, USA, david.c.folta@nasa.gov

The upcoming Lunar IceCube (LIC) mission will deliver a 6U CubeSat to a low lunar orbit via a ride-share opportunity during NASAs Artemis 1 mission. This presents a challenging trajectory design scenario, as the vast change in energy required to transfer from the initial deployment state to the destination orbit is compounded by the limitations of the LICs low-thrust engine. This investigation addresses these challenges by developing a trajectory design framework that utilizes dynamical structures available in the Bicircular Restricted Four-Body Problem (BCR4BP) along with a robust direct collocation algorithm. Maps are created that expedite the selection of invariant manifold paths from a periodic staging orbit in the BCR4BP that offer favorable connections between the LIC transfer phases. Initial guesses assembled from these maps are passed to a direct collocation algorithm that corrects them in the BCR4BP while including the variable low-thrust acceleration of the spacecraft engine. Results indicate that the ordered motion provided by the BCR4BP and the robustness of direct collocation combine to offer an efficient and adaptable framework for designing a baseline trajectory for the LIC mission.

1. Introduction

Advances in spacecraft technology miniaturization and an increase in launch opportunities have exponentially increased the number of CubeSats launched in the two decades since the platform was first proposed. Early success has motivated concept development for CubeSat missions beyond the bounds of low Earth orbit (LEO). In 2018, the two MarCO Cubesats, as the first to operate beyond Earth orbit, were deployed at Mars to monitor the entry, descent, and landing of the *Insight* lander.[1] Soon, thirteen CubeSats will utilize a rideshare opportunity on the Space Launch System (SLS) during the Artemis 1 mission to reach a variety of destinations well beyond LEO. Several of these spacecraft will reach heliocentric space, including the Near Earth Asteroid Scout (NEA Scout) and the CubeSat for Solar Particles (CuSP), with a flyby of a near-Earth asteroid and to investigate space weather, respectively. Other CubeSats on this launch which are destined for the Moon, include Lunar IceCube, Lunar Flashlight, and LunaH-Map. Together, these far-flung CubeSat missions indicate that small spacecraft will play an increasingly important role in space exploration.

While the CubeSat revolution has opened exciting opportunities, it brings new challenges. Despite technological advancements, ambitious CubeSat missions often require "doing more with less". For mission design, innovative trajectory design approaches are necessary that fully exploit natural dynamics. The Lunar IceCube (LIC) concept offers an excellent example of the challenges. This mission will deliver a 6U CubeSat to a low lunar orbit (LLO) where LIC will collect data on water transport throughout the lunar surface. A challenging trajectory design scenario emerges, as the vast change in energy required to transfer from the initial deployment state to LLO is compounded by the limited control authority of the LIC low-thrust engine. Furthermore, as a secondary payload, LIC is subject to changes in launch date and conditions required by the primary mission. These challenges necessitate a trajectory design strategy that is flexible and incorporates natural forces to assist with the required energy change.

This investigation proposes a trajectory design framework that addresses the challenges of the Lunar IceCube mission by utilizing dynamical structures available in the Bicircular Restricted Four-Body Problem (BCR4BP) along with a robust direct col-

location algorithm. Designing in the BCR4BP enables the gravitational force of the Sun to be leveraged to achieve part of the required energy change, while avoiding the additional perturbations of a full ephemeris model. A key feature of the proposed design approach is the use of a staging orbit near the Moon to split the trajectory into two phases: the first from spacecraft deployment to the staging orbit, and the second from the staging orbit to the science orbit. The focus on two separate arcs allows the two halves of the LIC trajectory to be designed mostly independently, thus, simplifying the redesign process if deployment conditions change. Moreover, a periodic orbit in the BCR4BP is employed as the staging orbit, to leverage its invariant manifolds for the design efficient of paths to and from the staging orbit. Another crucial component of the proposed framework is a direct collocation algorithm to correct initial guesses developed in the BCR4BP into optimal low-thrust trajectories. The robust convergence properties of direct collocation facilitate a wider variety of initial guesses despite large discontinuities in states or time. Together, these key design choices produce a design process that directly addresses the challenges of the Lunar IceCube mission. After an overview of the necessary background, the proposed trajectory design framework is described. Sample Lunar IceCube trajectories are constructed with the proposed strategies. While the trajectory design procedure is applied to the Lunar IceCube mission, it is sufficiently general for a wide variety of low-thrust missions especially those with limited control authority.

2. Background

2.1 Previous Work

First proposed in 2015, the Lunar IceCube (LIC) mission is a collaborative effort led by Morehead State University and supported by Goddard Space Flight Center (GSFC), Busek, and Catholic University of America[2]. During this mission the presence and movement of water in all its forms across a broad swath of the lunar surface is to be investigated. To enable the science collection, the 6U CubeSat will conduct science operations in a low lunar orbit (LLO) that covers a range of longitudes on the sunlit side of the Moon with a perilune altitude of 100 km. The full set of Keplerian orbital elements that define the science orbit are provided in Table 1 and are driven by the science requirements as well as the desire to maximize spacecraft lifetime while minimizing the station-keeping cost.[3] Station-keeping and the transfer trajectory to the science orbit are achieved via a

Table 1: Lunar IceCube science orbit Keplerian orbital elements defined in a Moon-centered inertial frame. Inclination is measured relative to the Moon's equator and the right ascension of the ascending node (RAAN) is defined with respect to the vernal equinox vector.

Orbital Element	Value
Semi-Major Axis, a	4271.4 km
Eccenctricity, e	0.5697
Inclination, i	89.35°
RAAN, Ω	65°
Argument of Periapsis, ω	355°

BIT-3 Busek ion thruster, which is capable of a maximum thrust of 1.24 mN, a specific impulse (I_{sp}) of 2640 seconds, and storing up to 1.5 kg of propellant.[4] Given the total 14 kg mass of LIC, these engine characteristics equip it with a maximum acceleration of 8.857×10^{-5} m/s^2. This value is compared to the maximum acceleration values of several other low-thrust spacecraft in Table 2; the low-thrust capability of LIC is clearly of the same order of magnitude as other recent or proposed low-thrust missions. The

Table 2: Representative low-thrust spacecraft acceleration levels.

Spacecraft	Max Acceleration (m/s^2)
Deep Space 1[5]	1.892×10^{-4}
Lunar IceCube	8.857×10^{-5}
Dawn[6]	7.473×10^{-5}
Gateway	3×10^{-5}

mission design challenge for Lunar IceCube is due less to the small thrust magnitude and more to the fact that this engine must deliver a massive change in energy to transfer from the high-energy deployment state near the Earth to the low-energy LLO. Despite this challenge, engineers at GSFC have developed a complete baseline trajectory, plotted in Figure 1, that utilizes the current launch date of June 25$^{\text{th}}$ 2020. However, this baseline trajectory must be redesigned when an updated launch date is released in the near future. Previous experience has demonstrated that varying the launch date can significantly impact the geometry of the LIC trajectory.

Faced with a challenging trajectory design scenario and uncertain launch conditions, engineers at GSFC have been informed by the results of several investigations on LIC trajectory design. A strategy that utilizes the high-fidelity General Mission Anal-

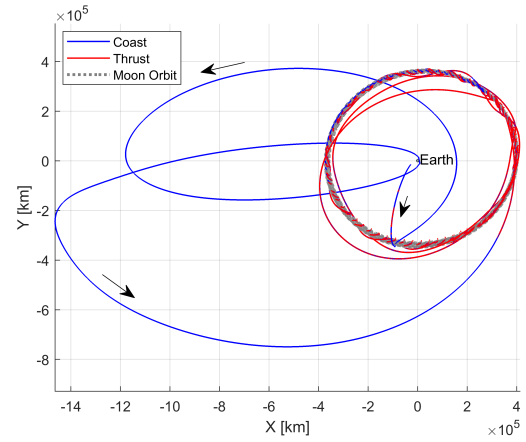

(a) Earth-Centered J2000 Inertial Frame

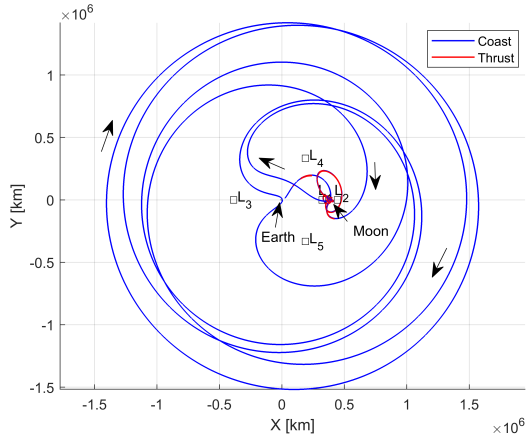

(b) Earth-Moon Rotating Frame

Fig. 1: Current baseline for Lunar IceCube trajectory developed assuming a June 25^{th}, 2020 launch date.

ysis Tool (GMAT) to design an LIC trajectory with a capture orbit at the Moon is offered by Mathur[7]. An innovative design approach for LIC is also presented by Bosanac, Folta, Cox, and Howell which subdivides the Lunar IceCube trajectory into three phases: deployment, phasing as well as energy adjustment, and lunar capture. A strategy for linking these phases that incorporates periapse maps and phasing arcs generated in the Sun-Earth Circular Restricted Three-Body Problem (CR3BP) or the BCR4BP is developed by Bosanac et al.[8–10]. Particular focus on the dynamics of the lunar capture phase is delivered separately by Folta et al.[11]. The strategy presented by Bosanac et al. is effective, and the current investigation expands upon their work by approaching the design problem with a framework that utilizes BCR4BP dynamical structures and direct collocation. This application may yield a design procedure that requires less computational time and is more robust with poor initial guesses.

In addition to work focused on LIC, this investigation is influenced by a greater body of literature on leveraging the influence of the Sun to design transfers from the Earth to the Moon. Belbruno and Miller demonstrate new types of Earth to Moon trajectories by simultaneously incorporating the gravitational influence of the Sun in addition to the Earth and Moon. Strategies for utilizing this acceleration to develop low-energy trajectories from the Earth to the Moon are developed by many authors, including Koon et al.[12], Gómez et al.[13], as well as Parker and Martin[14]. Low-energy trajectory design techniques are also applied to design low-thrust trajectories to the Moon by Mingotti et al.[15] and Zanottera et al.[16]. The present work uses direct collocation to compute low-thrust transfers building on the work of authors such as Enright and Conway[17] as well as Grebow, Ozimek, and Howell[18] who also employ this algorithm to generate low-thrust Earth to Moon transfers. Some authors exploring low-energy trajectory design also demonstrate transfers from Earth-Moon halo orbits to LLO, a strategy used in this investigation. Parker and Anderson[19] offer an impulsive transfer, while Mingotti et al. demonstrate a low-thrust result[20]. Recently, Cheng et al.[21] and Cao et al.[22] have more closely examined impulsive transfers from halo orbits to LLO in the CR3BP.

2.2 Bicircular Restricted Four-Body Problem

The BCR4BP builds on the assumptions of the CR3BP. The CR3BP models the path of a third body, P_3, under the influence of two more massive primary bodies, P_1 and P_2. These bodies are assumed to follow circular Keplerian orbits about their mutual barycenter, B_1. Additionally, the third body is assumed to possess negligible mass in comparison to the primary bodies, and this assumption is reasonable when the mass of the third body is quite small, e.g., a spacecraft. Finally, the mass ratio of P_1 and P_2 is denoted, $\mu = \frac{m_2}{m_1+m_2}$, and is used to characterize the CR3BP system.

The BCR4BP assumes the addition of a fourth body, P_4; both P_4 and the P_1-P_2 barycenter, B_1, move in circular orbits about their mutual barycenter, B_2. In this investigation, P_4 is always the Sun, thus the mass of P_4 equals the mass of the Sun, m_S. The circular orbits of P_1 and P_2 are not affected by the gravitational force of the Sun. As a result of this

assumption, the BCR4BP is *not coherent* because the motion of P_1 and P_2 are not influenced by the Sun, i.e., the indirect effects of the Sun are not incorporated. Additionally, as in the CR3BP, the mass of P_3 is assumed to be negligible relative to the other three bodies, i.e., $m_3 \ll m_2 < m_1 < m_S$. In general, the BCR4BP does not require that the Sun-B_1 orbit be coplanar with the P_1-P_2 orbit; however, in this investigation a coplanar model is employed. This model as well as a non-coplanar formulation are presented by Boudad[23].

It is insightful to examine motion in the BCR4BP from the perspective of two different rotating reference frames. The first is a reference frame rotating with P_1 and P_2, whose axes are defined by three orthogonal unit vectors. By convention, the $\hat{x}$ unit vector of this frame points from P_1 to P_2, while the $\hat{z}$ unit vector is parallel to the angular momentum vector of P_2 about P_1. Finally, the $\hat{y}$ unit vector is defined to complete the orthonormal set. A similar second rotating reference frame is defined for the Sun and B_1, but the $\hat{x}'$ unit vector is instead in the direction of B_1 from the Sun. Quantities expressed in the Sun-B_1 rotating frame are generally denoted with an apostrophe, e.g., x' is the x position coordinate of P_3 in the Sun-B_1 rotating frame. When the coplanar assumption is made, the orbit of the Sun as viewed from the P_1-P_2 rotating frame is modeled as illustrated in Figure 2. The position of the Sun in the

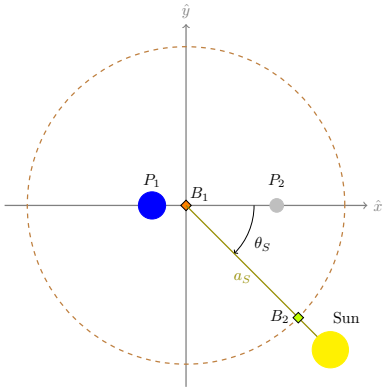

Fig. 2: Definition of the Sun angle in the Bicircular Restricted Four-Body Problem.

P_1-P_2 rotating frame is determined by the Sun angle, θ_S, and the distance from B_1 to the Sun is defined by the constant value a_S. Viewed from this frame, the Sun rotates clockwise about B_1, thus the value of θ_S decreases with time.

Motion in the BCR4BP is described by a set of differential equations similar to those of the CR3BP, but modified to accomodate the perturbing acceleration of the Sun. The P_1-P_2 rotating frame together with the Sun-B_1 rotating frame are commonly employed for analysis in the BCR4BP, and the equations of motion for P_3 may be expressed in either of these frames. The equations of motion for P_3, expressed in the P_1-P_2 frame and including a low-thrust force, are,

$$\ddot{x} = 2\dot{y} + \frac{\partial \Psi}{\partial x} + \frac{T_x}{m} \tag{1}$$

$$\ddot{y} = -2\dot{x} + \frac{\partial \Psi}{\partial y} + \frac{T_y}{m} \tag{2}$$

$$\ddot{z} = \frac{\partial \Psi}{\partial z} + \frac{T_z}{m} \tag{3}$$

$$\dot{m} = \frac{T}{v_e} \tag{4}$$

where the low-thrust force is represented by the three components of the thrust vector $\boldsymbol{T} = \{T_x \quad T_y \quad T_z\}$, and $||\boldsymbol{T}|| = T$. The magnitude of the thrust vector appears in Equation 4, along with the exhaust velocity, v_e. Together these parameters define the mass flow rate of the spacecraft, $\dot{m}$. Additionally, Ψ is the system pseudo-potential written in terms of P_1-P_2 rotating frames coordinates. This pseudo-potential and the pseudo-potential as expressed in Sun-B_1 coordinates, Ψ', are,

$$\Psi = \frac{1-\mu}{r_{13}} + \frac{\mu}{r_{23}} + \frac{1}{2}(x^2+y^2) + \frac{m_S}{r_{S3}} - \frac{m_S}{a_S^3}(x_S x + y_S y + z_S z) \tag{5}$$

$$\Psi' = \frac{1}{2}(x'^2+y'^2) + \frac{1-\mu_{SB_1}}{r'_{S3}} + \frac{\mu_{SB_1}(1-\mu_{P_1P2})}{r'_{13}} + \frac{\mu_{SB_1}\mu_{P_1P2}}{r'_{23}} \tag{6}$$

where the distance from the Sun to P_3 is represented by r_{S3}, and μ_{SB1} is the mass ratio of the Sun-B_1 system. Together these equations govern motion in the BCR4BP.

To facilitate numerical computation, the dependent variables in this dynamical model are nondimensionalized via a set of characteristic quantities. The values of the characteristic quantities are determined by the frame that the states are expressed in. When states are expressed in the P_1-P_2 rotating frame the characteristic length, l^*, is defined as the distance between P_1 and P_2; the characteristic mass, m^*, is equal to the combined mass of P_1 and P_2; and the characteristic time is determined such that the nondimensional angular velocity of P_1 and P_2 is equal to

one. The characteristic quantities are defined similarly when states are expressed in the Sun-B_1 rotating frame, except that the parameters of the Sun and B_1 replace those of P_1 and P_2 in the previous case. In this investigation, numerical propagation is performed using the equations of motion expressed in the P_1-P_2 rotating frame.

In contrast to the CR3BP, the BCR4BP is not an autonomous system, i.e., motion in this model is time dependent. As a consequence, this system possesses no integral of the motion. However, the Hamiltonian, serves as a useful metric for analyzing the motion of P_3 in the BCR4BP. The Hamiltonian defined in this investigation does not include the low-thrust force, thus it represents only the total ballistic energy of the system. The Hamiltonian may be computed using coordinates expressed in either the P_1-P_2 or Sun-B_1 rotating frames.

$$H = 2\Psi - (\dot{x}^2 + \dot{y}^2 + \dot{z}^2) - \sigma \tag{7}$$

$$H' = 2\Psi' - (\dot{x}'^2 + \dot{y}'^2 + \dot{z}'^2) \tag{8}$$

If P_1 and P_2 are the Earth and Moon, respectively, the resulting Hamiltonian values are adjusted to be similar in magnitude to the Jacobi constant values in either the Earth-Moon or Sun-Earth CR3BP models. The value of H is scaled by a constant parameter σ that is incorporated to offset the high value terms introduced by the Sun and ensure that H is of a similar magnitude to the Jacobi constant value of the Earth-Moon CR3BP. Throughout this analysis, $\sigma = 1690$ nondimensional units.

The Hamiltonians defined in Equations 7 and 8 represent the total ballistic energy of the system because they do

The same types of dynamical structures that are available in the CR3BP also emerge in the BCR4BP, namely, periodic and quasi-periodic orbits as well as their invariant manifolds. Because the BCR4BP is non-autonomous, these structures are not only defined by position and velocity states, but also by specific epochs, i.e., Sun angles. A periodic orbit in the BCR4BP requires a repetition of the same position and velocity states at the same Sun angle. This angle requirement implies that all periodic orbits in the Sun-Earth-Moon BCR4BP possess a resonance with the synodic period of the Sun, approximately 29.5 days. The Sun angle, θ_S, completes a full revolution once every synodic period. For example, a periodic halo orbit in the Sun-Earth-Moon BCR4BP, and computed about the Earth-Moon L_2 libration point, is displayed in Figure 3. This orbit possesses a 2:1 synodic resonance, that is, two revolutions along the

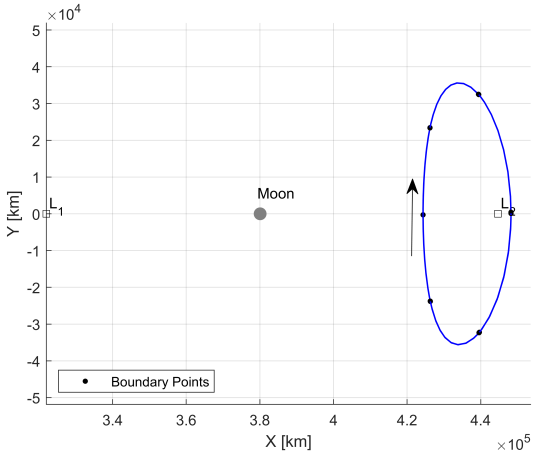

Fig. 3: 2:1 synodic resonance halo orbit in the Sun-Earth-Moon BCR4BP computed about the Earth-Moon L_2 libration point. This orbit is used as a staging orbit in the proposed design framework. Projected in the xy-plane of the Earth-Moon rotating frame.

halo orbit are completed for every one synodic period. Similarly, the individual trajectories along the invariant manifold associated with a periodic orbit in the BCR4BP are associated with unique Sun angles. Every path along a stable or unstable manifold arrives at or departs from the periodic orbit at a specific Sun angle. Structures available in the BCR4BP can appear similar to those in the CR3BP, but the dependency on Sun angle is critical.

2.3 Direct Collocation

Low-thrust trajectory design is frequently posed as a continuous optimal control problem; at each instant in time a thrust vector is selected that minimizes a cost, typically propellant consumption, time of flight, or some combination. A multitude of strategies for solving continuous optimal control problems are available, and the best strategy is dependent on the characteristics of the problem. In this investigation, a direct optimization technique is employed because these methods are generally more robust to poor initial guesses than indirect optimization formulations and require less computational time than global optimization approaches. This balance of robustness and efficiency is critical for the proposed design framework which aims to rapidly explore a large search space of potential LIC trajectory solutions.

The process of discretizing a continuous optimal control problem to allow a numerical solution is de-

noted transcription, and collocation offers one approach to this procedure. A collocation scheme uses polynomials to approximate a solution to the set of differential equations that govern a dynamical model, for example, Equations (1)-(3). A collocation problem is discretized into n segments where the dynamics along each segment are approximated by a polynomial of degree N. Many options are available, however this investigation employs 7^{th} degree Legendre Gauss polynomials. The polynomial for each segment is constructed from $(N+1)/2$ variable nodes, $\boldsymbol{x}_{i,j}$, where $i = 1, \ldots, n$, and $j = 1, \ldots, N$. Each segment also contains $(N-1)/2$ defect nodes where the error between the equations of motion and the polynomial approximation is calculated. This error is iteratively reduced by manipulating the states corresponding to the variable nodes in an update process informed by the gradient of the problem constraints with respect to the states. Collocation is the transcription method of choice in this investigation due to its wide basin of convergence and amenability to the addition of constraints. Collocation often exhibits a wider basin of convergence than other approaches for solving a system of differential equations, i.e., it will converge upon a solution despite a poor initial guess, even when other methods fail. Since this investigation utilizes direct optimization, the overall optimization approach employed here is termed *direct collocation*.

The specific tool to implement direct collocation for this investigation is labelled COLT (Collocation with Optimization for Low-Thrust) and was developed in collaboration with Daniel Grebow at the Jet Propulsion Laboratory[24,25]. The direct collocation framework in COLT generally follows the scheme developed by Grebow and Pavlak and implemented in their MColl software[26]. The variables and constraints generated by the collocation problem, as well as those unique to low-thrust trajectory optimization, are based on a design variable and constraint scheme.[27] The design variable vector, $\boldsymbol{X}$, is arranged in COLT such that the variables corresponding to each segment are grouped together, i.e.,

$$\begin{aligned}\boldsymbol{X} = \big[&\boldsymbol{u}_1 \quad m_{0,1} \quad m_{f,1} \quad \boldsymbol{x}_{1,1} \quad \boldsymbol{x}_{1,3} \\ &\boldsymbol{x}_{1,5} \quad \boldsymbol{x}_{1,7} \quad \ldots \quad \boldsymbol{u}_n \quad m_{0,n} \\ &m_{f,n} \quad \boldsymbol{x}_{n,1} \quad \boldsymbol{x}_{n,3} \quad \boldsymbol{x}_{n,5} \quad \boldsymbol{x}_{n,7}\big]^T\end{aligned} \tag{9}$$

Equation (9) offers a sample design variable vector when the polynomial degree is $N = 7$, leading to four variable nodes, $\boldsymbol{x}_{i,j}$, per segment. Furthermore, the variable node states are vectors of position and velocity states, i.e., $\boldsymbol{x}_{i,j} = [\boldsymbol{r}_{i,j}, \ \dot{\boldsymbol{r}}_{i,j}]^T$. The vector $\boldsymbol{u}_i$ contains control variables for the i^{th} segment, while $m_{0,i}$ and $m_{f,i}$ are the initial and final mass for each segment. Numerous options are available for parameterizing the control in a low-thrust trajectory optimization problem, and some schemes possess favorable numerical properties. In COLT, the control variables are the three components of the thrust unit vector, $\boldsymbol{u}_i = [\hat{T}_1, \hat{T}_2, \hat{T}_3]^T$. These variables are then constrained such that $||\boldsymbol{u}|| = 1$. The magnitude of the thrust vector, T, is computed using the initial and final mass along each segment. The maximum magnitude of the thrust vector is T_{max}, and this quantity along with the I_{sp} define the maximum mass flow rate, $\dot{m}_{max}$. Initial and final mass, $\dot{m}_{max}$, and a timespan, Δt_i, are employed to compute a throttling value, s_i, for each segment that is constrained to the range $0 \leq s_i \leq 1$,

$$s_i = \frac{m_{0,i} - m_{f,i}}{\dot{m}_{max,i} \Delta t_i} \tag{10}$$

The throttling value evaluated with Equation (10) delivers the thrust magnitude, $T_i = s_i T_{max,i}$, and the mass flow rate, $\dot{m}_i = s_i \dot{m}_{max,i}$, for a given segment. The maximum mass flow rate, $\dot{m}_{max,i}$, and maximum thrust magnitude, $T_{max,i}$, correspond to the selected low-thrust engine model, thus, these variables are either constant values or functions of an expression that incorporates additional parameters, such as power and distance from the Sun. The elements of the design variable vector are updated throughout the optimization process and, at each iteration, these variables are employed to evaluate the problem constraints.

A variety of problem constraints are available in COLT. While some must be enforced to obtain a solution to the low-thrust trajectory optimization problem, others are only included for specific scenarios. Within the COLT algorithm, these constraints are arranged into equality constraints, $\boldsymbol{F}_{eq}$, and inequality constraints, $\boldsymbol{F}_{ineq}$.

$$\boldsymbol{F}_{eq} = \begin{bmatrix}\boldsymbol{g}_{defect} & \boldsymbol{g}_{continuity} & \boldsymbol{g}_{\hat{T}} & \boldsymbol{\psi}_0 & \boldsymbol{\psi}_f\end{bmatrix}^T \tag{11}$$

$$\boldsymbol{F}_{ineq} = \begin{bmatrix}\boldsymbol{g}_s & \boldsymbol{g}_{rad}\end{bmatrix}^T \tag{12}$$

Equations (11) and (12) illustrate the organization of common constraints utilized within COLT. A collocation scheme always enforces defect constraints, $\boldsymbol{g}_{defect}$, to produce a valid solution. Because of the selected node spacing scheme, COLT also requires the enforcement of continuity constraints between segments, $\boldsymbol{g}_{continuity}$, as do some other collocation im-

plementations. Additionally, constraints on the controls are included to ensure that, for each segment, the control variable vector possesses unit magnitude, $\boldsymbol{g}_{\hat{T}}$, and the throttle value is between 0 and 1, $\boldsymbol{g}_s$. All other constraints are optional and problem specific. For example, it is frequently beneficial to include minimum radius constraints with respect to gravitational bodies, $\boldsymbol{g}_{rad}$. This constraint enforces a "keep-out" zone around these bodies such that the trajectory remains beyond the zone. Other useful constraints include constraining the states, energy, and/or orbital elements for the initial, $\boldsymbol{\psi}_0$, and final, $\boldsymbol{\psi}_f$, boundary points along a trajectory arc. Specific low-thrust trajectory design scenarios may require other constraints, and these are straightforward to incorporate in a collocation framework.

Several additional features of COLT are available in the current version of the algorithm. The design variable and constraint framework for implementing collocation is paired with the optimizer IPOPT[28] to compute mass optimal low-thrust trajectories. For a more tractable optimization problem, the design variables are frequently bounded within a desired range. Some design variables possess obvious upper and lower bounds; for example, necessary constraints on the control and mass variables are enforced simply by applying bounds. Bounds on other variables, such as the position and velocity states, are defined relative to their initial values and are defined as user inputs. Convergence to an optimal solution is also aided by the ability to scale the design variables and constraints. Finally, collocation is typically paired with a mesh refinement scheme to generate a sufficiently accurate solution. Mesh refinement schemes adjust the spacing of boundary points along a solution to evenly distribute and ultimately reduce error. The mesh refinement strategies leveraged in this investigation, developed by Grebow and Pavlak, are labelled Control Explicit Propagation (CEP) and Hybrid CEP.[26] Bounding the design variables, scaling the problem, and conducting mesh refinement ensure that COLT is a robust and efficient direct collocation algorithm.

2.4 Nearest Neighbor Search

The proposed trajectory design framework employs maps to aid the construction of initial guesses that are passed to the direct collocation algorithm. Maps capture the returns of trajectory segments to a particular hyperplane, Σ. Frequently, maps are used to facilitate the identification of close connections between two sections of a spacecraft trajectory, e.g., one propagated forwards in time and the other backwards. Points along these two trajectory segments that intersect the selected hyperplane are displayed on the map. Example hyperplanes include, a plane in configuration space, e.g., the xy-plane, or the occurrence of a specific epoch. In this investigation the Sun angle, θ_S, is used to define hyperplanes for two different maps. Parameters such as position, velocity, or energy at the hyperplane intersections may be displayed on the map. The maps in this analysis include points, i.e., hyperplane crossings, from many trajectories, and each trajectory can possess multiple returns to the hyperplane. Due to the large number of points and multiple dimensions of each point plotted on the map it can be challenging to visually identify the best connections between trajectory segments. Therefore, a nearest neighbor search algorithm aids the identification of points on maps that share similar characteristics.

Nearest neighbor (NN) algorithms are employed in many fields of computer science under a variety of names.[29] Fundamentally, the nearest neighbor problem involves locating the point p in a set of points P with the shortest distance to a given point q, assuming all points occupy a space of dimension d.[30] In the present application, events along the forward propagated group of trajectories provide one set of points, while events on the backwards propagated trajectories comprise the other set. Thus, an NN search is ideally suited for identifying close connections between events recorded on maps. The tool *Poincare*, developed at JPL, employs NN algorithms for this purpose.[31] In this investigation, Matlab's `knnsearch` algorithm is employed for the NN search. Furthermore, a standardized Euclidean distance metric is used to compute the distances between points. The scaling for the standardization of the distance metric as well as the exact parameters passed to the NN search routine are defined in the formulation of the design framework. The NN search algorithm is a useful tool that complements visual inspection of maps to identify close connections between trajectory segments.

3. Trajectory Design Framework

The proposed trajectory design framework is distinguished by three key features: modeling in the BCR4BP, employing a staging orbit, and computing low-thrust transfers with direct collocation. Together these design choices deliver a flexible and robust procedure for constructing the Lunar IceCube trajectory. A staging orbit near the Moon is used to

divide the mission design challenge into two phases, as illustrated in Figure 4. Phase 1 occurs from de-

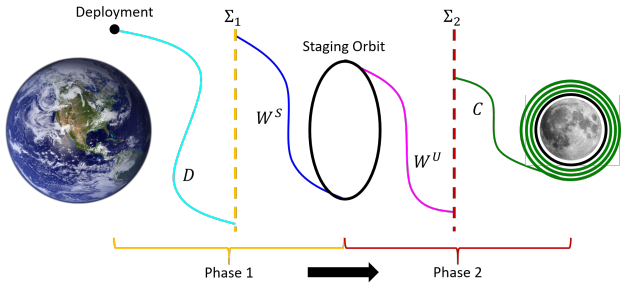

Fig. 4: Schematic of trajectory design framework.

ployment to the staging orbit and Phase 2 passes from the staging orbit to the low lunar altitude science orbit. These two phases are solved nearly independently where the spacecraft mass is the only parameter, aside from the selected staging orbit, carried over between phases. In the BCR4BP, any discrepancies in epoch between the two phases are overcome simply by waiting in the staging orbit until the desired departure epoch is reached. Initial guesses for both phases of the trajectory design framework are assembled with the aid of two different maps. These maps display intersections with the hyperplanes Σ_1 and Σ_2 which are defined by the Sun angles θ_{S_1} and θ_{S_2}, respectively. The first map captures intersections of Σ_1 by forward propagated deployment trajectory arcs, D, and backward propagated paths on the stable manifold of the staging orbit, W^S. Similarly, the second map captures intersections of Σ_2 by forward propagated trajectories on the unstable manifold of the staging orbit, W^U, and backward propagated capture trajectory arcs, C. Close matches between hyperplane intersections of forward and backward propagated trajectories segments are identified and their corresponding trajectory segments are assembled into an initial guess for the direct collocation tool COLT.

3.1 Phase 1: Deployment to Staging Orbit

Design of Phase 1 of the Lunar IceCube trajectory is facilitated by the creation of maps that display events along trajectories propagated forward from deployment and backward on the stable invariant manifold of the staging orbit. To expand the options available on these maps a range of forward and backward propagated trajectories are generated. Different trajectories on the staging orbit's stable manifold, W^S, are obtained by changing the state and epoch of the departure point from the periodic orbit. In contrast, because the deployment state and epoch cannot be changed, a span of forward propagated trajectories is generated by varying thrust direction prior to the first Lunar flyby. The deployment state and epoch used in this investigation are the same as those used to generate the baseline trajectory displayed in Figure 1.

Trajectories propagated forward in time from the deployment condition are divided into three parts, an initial coast period, a thrust segment, and a second coast period. An example of this subdivision is displayed in Figure 5. The duration of the first coast

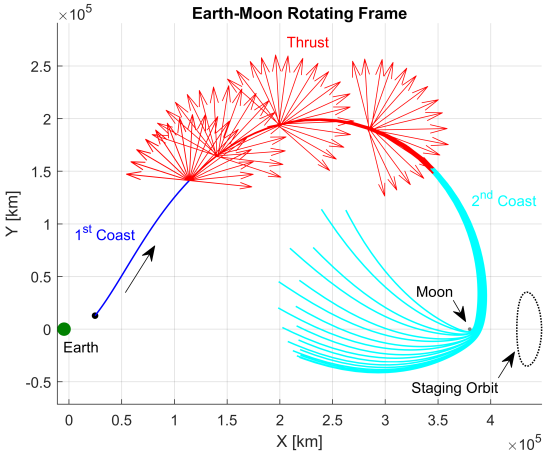

Fig. 5: Sample range for deployment trajectories in the creation of a Phase 1 map, plotted in the Earth-Moon rotating frame. The first coast period is 0.8 days, the thrust segment is 3 days, and the second coast section is 4 days. Thrust vectors span a range of α angle vales from 0 to $3\pi/2$ in the VNB frame. Trajectories that impact the Moon are omitted.

segment is set to 0.8 days and is dictated by the time required to perform initial spacecraft systems checkouts and obtain tracking data. Following this coasting period, a multi-day thrust segment is introduced. A thrust segment of three days is used in this investigation; however, this value can be altered to change the post-flyby behavior of the deployment trajectory. The direction of the thrust vector along this segment is varied over a user-defined span of angles to generate a range of deployment trajectories. The angle, α, used to determine the thrust vector direction is defined relative to the $\hat{v}$ unit vector in the velocity-normal-binormal (VNB) frame. This frame is defined such that the $\hat{v}$ unit vector is in the direction of the velocity vector of the spacecraft expressed in the ro-

tating frame. Additionally, the $\hat{n}$ unit vector is in the direction of the spacecraft's angular momentum vector relative to B_1, and the $\hat{b}$ unit vector is defined to complete the orthonormal set. The angle α determines the direction of the thrust vector in the vb-plane, and no out-of-plane, i.e., $\hat{n}$ component of the thrust vector, is introduced. By varying α from α_{min} to α_{max} many different post-flyby trajectories are generated, as seen in Figure 5. In this investigation, $\alpha_{min} = 0$ and $\alpha_{max} = 270°$. Following the thrust segment a second coast segment is propagated for a user-defined number of days. Intersections of this section of trajectory with the hyperplane Σ_1 are recorded and used to generate the map.

Trajectories propagated backward in time along the stable manifold of the staging orbit are linked to the forward propagated deployment trajectory. The stable invariant manifolds of periodic orbits offer efficient paths onto the orbits. Thus, using these trajectories to guide LIC to the staging orbit should lead to a solution that requires less propellant than other potential insertion paths. Figure 6 displays trajectories along the stable manifold. The initial trend

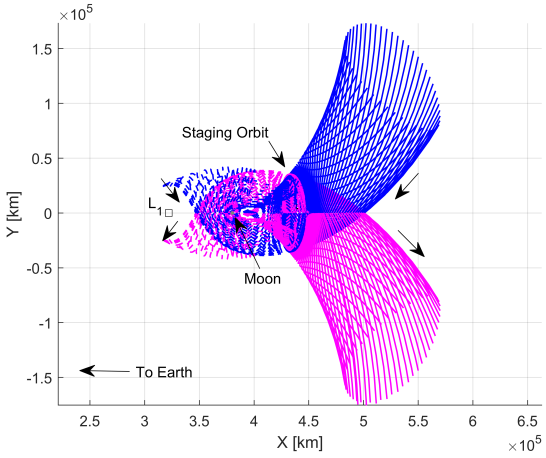

Fig. 6: Stable (blue) and unstable (magenta) manifold trajectories of 2:1 resonant L_2 halo orbit in the BCR4BP plotted in the Earth-Moon rotating frame. Solid lines indicate a positive stepoff direction and dashed lines correspond to a negative stepoff direction.

of these manifold paths is either in the positive or negative x direction. In the former case, trajectories on the manifold tend to escape the Earth-Moon system, and these paths offer more useful connection points with the trajectories propagated forward from deployment. Stepping off the periodic orbit and onto the stable manifold at different states and epochs around the orbit generates a variety of manifold paths.

A map is created to join the two halves of the Phase 1 LIC trajectory by recording intersections of the deployment trajectories and the paths on the stable manifold with Σ_1. Trajectories are propagated until either a maximum time limit or a maximum distance from the Earth is reached. In this case, a maximum time of 100 days and a maximum Earth distance of 3×10^6 km are used for both the deployment and manifold propagation. An example map is displayed in Figure 7 where the Sun angle at which events are recorded is $\theta_S = 135°$. The events that occur along

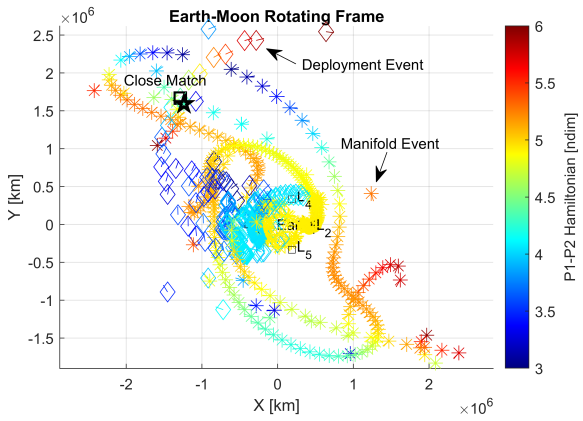

Fig. 7: Map of Σ_1 intersections of the deployment trajectory and paths along the stable manifold of the staging orbit in the BCR4BP. Intersections are projected in the xy-plane of the Earth-Moon rotating frame, and the Sun angle selected for Σ_1 is 135°.

the deployment trajectory are plotted as diamonds while the events on the stable manifold are marked as asterisks. All events are plotted in the Earth-Moon rotating frame, and each marker is colored according to the Hamiltonian, H, of the spacecraft at the time of the event. Additionally, the spacecraft's xy-plane velocity direction is plotted as an arrow centered at the marker. Adding this extra information to each plot aids the identification of close matches between deployment and manifold trajectories. By selecting events that match closely in position space along with energy and velocity direction useful initial guesses for the direct collocation algorithm can be obtained. A close match, identified by the nearest neighbor algorithm, is highlighted in Figure 7. The deployment

and manifold trajectories are propagated to the selected event times and used as an initial guess for the direct collocation algorithm in the Sample Trajectory Design section.

3.2 Phase 2: Staging Orbit to Science Orbit

Phase 2 of the LIC trajectory consists of the transfer from the staging orbit to the science orbit. An initial guess for this phase is assembled in a similar manner to Phase 1; events along a range of forward and backward propagated trajectories are plotted on a map used to select the initial guess. In this case, paths along the unstable manifold, W^U, of the staging orbit make up the forward propagated trajectory segments. The backwards propagated segments consist of trajectories propagated with low-thrust, in reverse time, from different true anomaly values on the science orbit. The map used to link the forward and backward propagated trajectories again consists of Sun angle events along each trajectory segment plotted in the xy-plane.

Trajectories along the unstable manifold of the staging orbit offer energy efficient paths for departing the orbit and beginning the spiral down to the science orbit. Apart from their inverse direction these trajectories behave similarly to those on the stable manifold and are displayed in Figure 6. Paths on the unstable manifold offer a variety of locations and epochs at which to depart the staging orbit, and Sun angle events along these trajectories populate the Phase 2 map.

To generate a variety of trajectories that insert onto the final orbit, backwards propagation is initiated from true anomaly values on the orbit that span the full 360° range. The backwards propagation assumes a maximum thrust anti-velocity control law - that is, the thrust vector is always oriented along the $-\hat{v}$ direction of the VNB frame and has a magnitude equal to the maximum thrust of LIC. Recall that the VNB frame is defined relative to the rotating frame velocity vector. Application of this control law produces a trajectory that, in forward time, gradually spirals down to the final science orbit, as shown in Figure 8(a). The backwards propagated trajectories must assume an epoch for insertion onto the science orbit as well as a spacecraft mass at insertion. Reasonable inferences for these values made during initial guess formulation are later adjusted by the direct collocation algorithm to ensure a continuous final result. Previous analyses have indicated that the total duration of the LIC transfer is approximately one year, thus a date of June 1st, 2021 is used to obtain a Sun

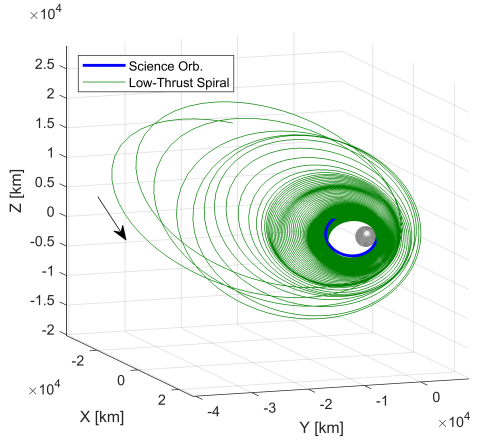

(a) Single backwards propagated trajectory in the Moon-centered J2000 inertial frame.

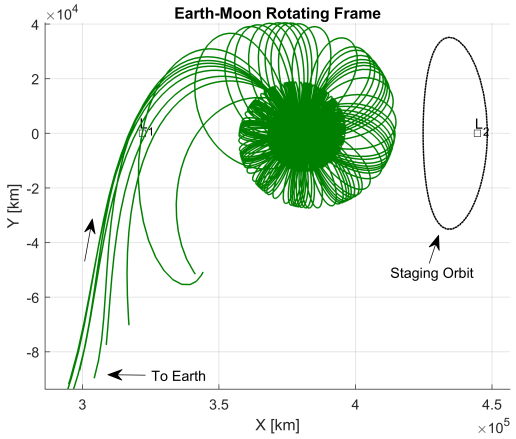

(b) Multiple backwards propagated trajectories in the Earth-Moon rotating frame generated by initiating propagation at different true anomaly values on the science orbit.

Fig. 8: Backwards propagation from the science orbit with a constant maximum thrust anti-velocity thrust vector.

angle at science orbit insertion (SOI) of 105.7°. Similarly, earlier investigations indicate that, at most, LIC consumes half of the available propellant mass to execute the transfer from deployment to science orbit, therefore a final mass at SOI of 13.25 kg is assumed. Even if intuition for the epoch and mass at SOI is not available, the robustness of the direct collocation algorithm increases the likelihood that poor estimates for these values can still produce useful initial guesses. While these two quantities are constant for all backwards propagated trajectories, using a range of true anomaly values to initialize propagation ensures that each trajectory evolves differently, as seen in Figure

8(b). Trajectories are propagated until either a maximum time limit or a maximum distance from the Earth is reached. In this case, manifold trajectories are propagated for a maximum time of 100 days while the backward propagated low-thrust spiral is propagated for a maximum time of 200 days. Both types of trajectories are propagated to a maximum distance from the Earth of 6×10^5 km. Sun angle events along each propagated trajectory are recorded and added to the Phase 2 map.

Events along the forward and backward propagated trajectory segments generated for Phase 2 are projected on the xy-plane and colored according to their H value. These three parameters along with the angle of the velocity vector with respect to the x-axis in the xy-plane are used to identify close matches between trajectory segments. The event used in this case is once again the occurrence of a desired Sun angle. An example map is displayed in Figure 9(a) where the Sun angle at which events are recorded is 75°. The events that occur along the backward propagated trajectory are plotted as diamonds while the events on the unstable manifold are displayed as stars. By selecting events that match closely in position space along with energy and velocity direction, suitable initial guesses for the direct collocation algorithm are obtained. A close match, identified by the nearest neighbor algorithm, is highlighted in Figure 9(b). The deployment and manifold trajectories propagated to the selected event times are used as an initial guess for the direct collocation algorithm in Section 4.

Modifications are made to COLT's nominal collocation scheme to enable design of a continuous low-thrust transfer from the staging orbit to the final science orbit for LIC. The low-thrust spiral required to transfer between these two orbits is long and includes many revolutions. This type of trajectory is challenging to optimize using the collocation framework implemented in COLT, which employs Cartesian coordinates. Other collocation schemes that utilize modified equinoctial elements (MEE) have successfully optimized low-thrust spiral trajectories.[32,33] However, rather than implement a complex multi-phase collocation scheme that uses Cartesian and MEE coordinates, a simplified approach is used. This strategy divides Phase 2 into two halves: one that is solved with direct collocation and the other which is explicitly propagated backwards in time from science orbit insertion (SOI).

The backwards propagated section of the LIC trajectory is updated in the differential corrections process by the addition of three design variables and a constraint. The three design variables are appended to the design variable vector in Equation (9),

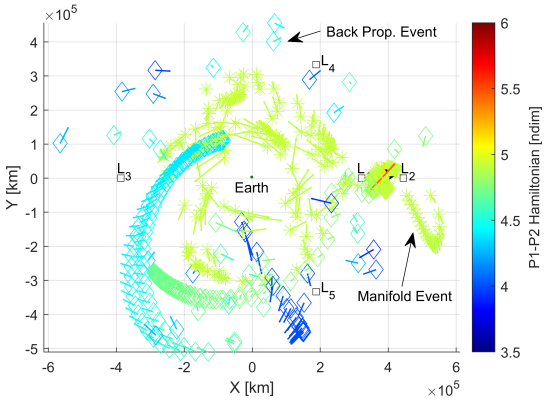

(a) Earth-Moon Rotating Frame

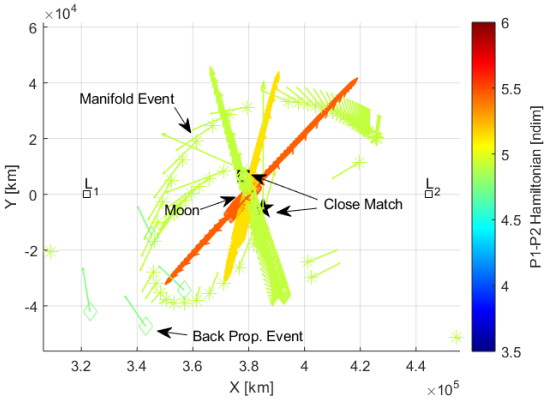

(b) Zoomed View of Phase 2 Map

Fig. 9: Map of Sun angle events along unstable manifold trajectory and low-thrust spiral to the science orbit in the BCR4BP.

$$\boldsymbol{X}_{spiral} = \begin{bmatrix} \boldsymbol{X} & \tau_{spiral} & \nu_{SOI} & m_{SOI} \end{bmatrix} \tag{13}$$

where τ_{spiral} is the backwards propagation time from SOI, ν_{SOI} is the true anomaly value on the science orbit at insertion, and m_{SOI} is the spacecraft mass at SOI. By including these variables in the corrections process, the evolution of the spiraling LIC trajectory is allowed to change and can be joined with the section of the transfer that departs from the staging orbit. A constraint is added to ensure that the two halves of this connect,

$$\boldsymbol{g}_{spiral} = \boldsymbol{x}_{n,f} - \boldsymbol{x}_{spiral,f} \tag{14}$$

where $\boldsymbol{x}_{n,f}$ is the final state in the final segment of the LIC trajectory section that is represented by collocation polynomials, and $\boldsymbol{x}_{spiral,f}$ is the state at the end of the backwards propagation from the science orbit. Using the design variables in equation (13) and the constraints in equations (11), (12), and (14), a single direct collocation problem is solved. The solution is a continuous low-thrust transfer from the staging to the science orbit. Because a sub-optimal control law is used for the spiraling portion of the trajectory, the result of the direct collocation algorithm is not a fully optimized low-thrust transfer. However, optimization is used to minimize the propellant consumed before the backwards propagated spiraling phase begins. Additionally, the selected control law ensures the maximum rate of change of the spacecraft's energy, and this reduces the time required to achieve Lunar capture, thus reducing propellant consumption. This approach for computing a trajectory from the staging to the science orbit generates a continuous low-thrust transfer without the complexity of a multi-phase collocation scheme.

4. Sample Trajectory Design

The proposed trajectory design framework offers a procedure for developing an initial guess for the full Lunar IceCube trajectory, from deployment to insertion on the science orbit. After maps are generated for phases 1 and 2, close matches between forward and backward propagated trajectory segments are identified and used to construct an initial guess for the direct collocation algorithm. This robust algorithm is frequently able to converge even when given very discontinuous initial guesses.

4.1 Phase 1: Deployment to Staging Orbit

An initial guess for Phase 1 of the Lunar IceCube trajectory is assembled by identifying a close match between events on deployment and stable manifold trajectories in a Phase 1 map. An example of such a match is highlighted by black markers in Figure 7, where the black square indicates the deployment event and the black five-pointed star denotes the manifold event. This match is identified using the nearest neighbor search algorithm and the trajectories that correspond to the selected events are shown in Figure 10. While a discontinuity between the forward and backwards propagated trajectories is evident, the criteria used to identify matches between events on the map yield a promising initial guess. This initial guess is passed to COLT which eliminates the discontinuity by inserting additional thrust segments. The optimized trajectory resulting from this initial guess, is displayed in Figure 11, and consumes 0.23 kg of propellant to reach the staging orbit in 140 days. The collocation algorithm computes this solution with relatively few iterations, moreover the geometry of the initial guess is generally preserved in the direct collocation result. These two factors indicate that the initial guess identified with the Phase 1 map was useful in guiding the algorithm towards a solution.

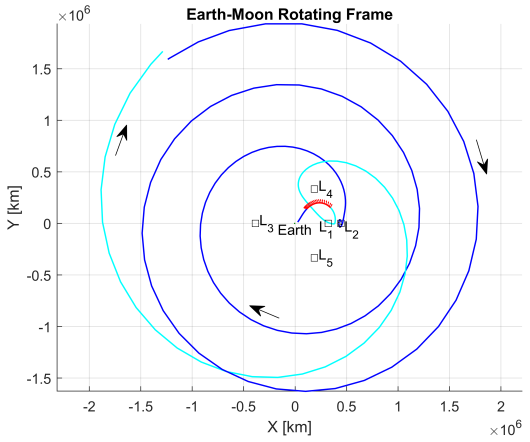

(a) Earth-Moon Rotating Frame

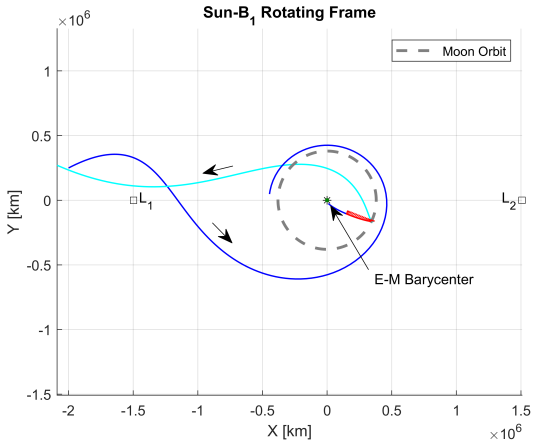

(b) Sun-B_1 Rotating Frame

Fig. 10: Initial guess for Phase 1 trajectory. Corresponds to the close match identified in the Phase 1 map in Figure 7.

The strong influence of the initial guess on the final result is more evident when alternate solutions are examined. A different Phase 1 map, one generated with events at a Sun angle of 180°, is used to construct the initial guess shown in Figure 12. This

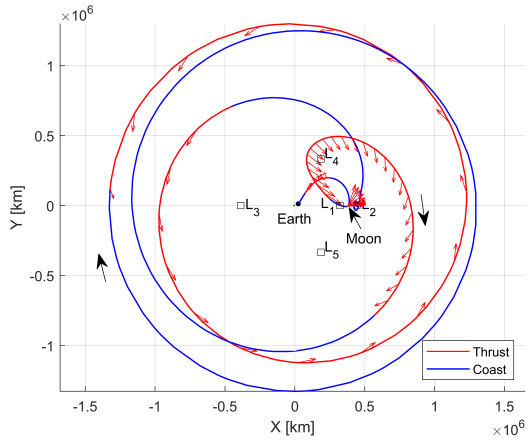

(a) Earth-Moon Rotating Frame

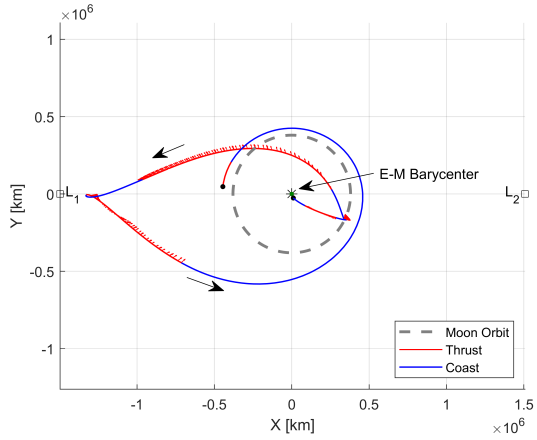

(b) Sun-B_1 Rotating Frame

Fig. 11: Direct collocation result for Phase 1 transfer using initial guess displayed in Figure 10. This transfer takes 140 days and consumes 0.23 kg of propellant.

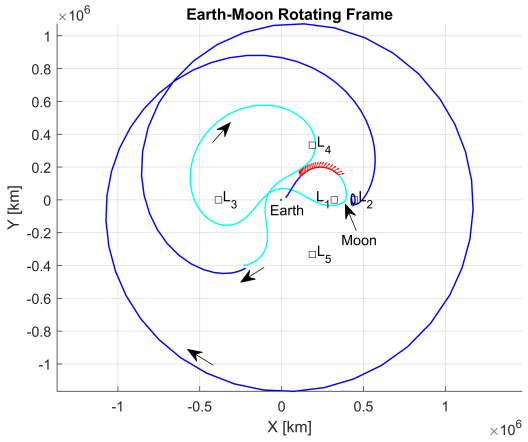

(a) Earth-Moon Rotating Frame

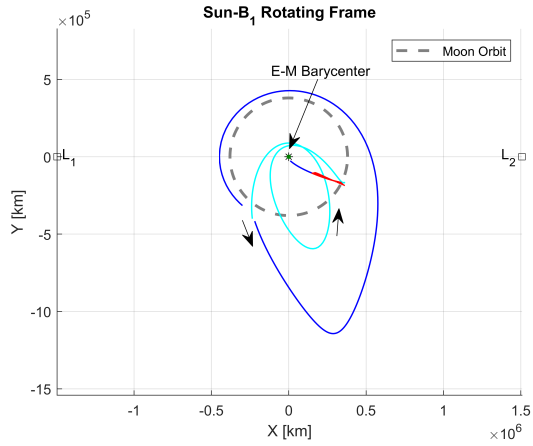

(b) Sun-B_1 Rotating Frame

Fig. 12: Initial guess for Phase 1 trajectory that includes an Earth flyby. Corresponds to a close match identified in a Phase 1 map generated with events recorded at a Sun angle of 180°.

initial guess includes an Earth flyby, and this flyby is maintained in the optimized COLT solution displayed in Figure 13. This transfer reaches the staging orbit in approximately 115 days and requires only 0.09 kg of propellant mass. By experimenting with maps generated using different Sun angle events and selecting various event pairs on those maps, a variety of initial guess geometries can be obtained that lead to an array of optimized solutions. The flexibility of this approach and the diversity of solutions it offers makes it adaptable to different mission constraints and deployment conditions.

4.2 Phase 2: Staging Orbit to Science Orbit

A solution for Phase 2 of the LIC trajectory is computed in a similar manner to Phase 1, and because a staging orbit is used, no information on the converged results of Phase 1 is required to develop an initial guess for Phase 2. A close match between events on a sample Phase 2 map is identified in Figure 9, and the trajectories corresponding to the selected events are displayed in Figure 14(a). Because the staging orbit and the science orbit are significantly out-of-plane, the xy-plane view of the Phase 2 map shown in Figure 9 can be deceptive. Events that appear to overlap in this map may differ significantly when the $\hat{z}$ position and velocity components are considered.

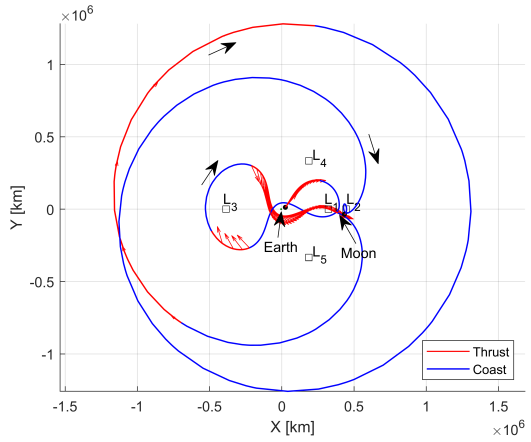

(a) Earth-Moon Rotating Frame

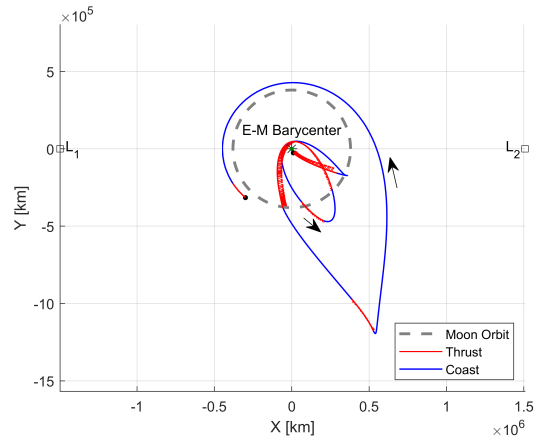

(b) Sun-B_1 Rotating Frame

Fig. 13: Direct collocation result for Phase 1 transfer using initial guess displayed in Figure 12. This transfer takes 115 days and consumes 0.09 kg of propellant.

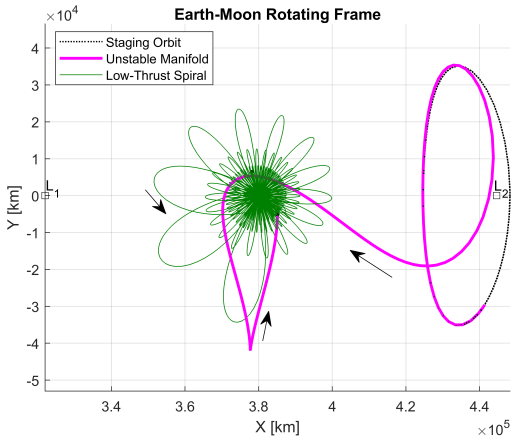

(a) Initial Guess

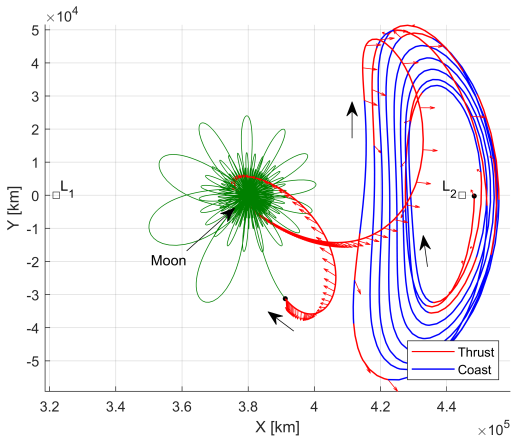

(b) Converged Result

Fig. 14: Initial guess and direct collocation result for Phase 2 transfer in the Earth-Moon rotating frame that remains in the Lunar vicinity. This transfer takes 228 days and consumes 0.52 kg of propellant.

As a result, the NN search algorithm is especially useful for identifying matches on Σ_2, because the algorithm can be weighted to emphasize close matches in energy, a parameter that includes information on the out-of-plane components of each event. This step enables the identification of useful initial guesses that would likely have been passed over if visual inspection alone were employed. The close connection point between the unstable manifold and low-thrust spiral trajectories displayed in Figure 14(a) actually occurs under the Moon, i.e., $z < 0$, therefore it is difficult to see even in the zoomed in view of the Phase 2 map shown in Figure 9(b). Utilizing the nearest neighbor algorithm ensures that this close match is not overlooked.

The initial guess identified with the Phase 2 map and NN search is passed to the direct collocation algorithm, i.e., COLT, for convergence. In general, it is more difficult to achieve convergence for this phase of the LIC trajectory because the initial guesses generated by the map possess larger state discontinuities and the majority of the trajectory is near the Moon which increases the sensitivity of the optimizer. The likelihood of convergence is increased by bounding the design variables, scaling, and including a minimum radius constraint with respect to the Moon. Additionally, convergence is improved by providing

COLT more trajectory, and therefore more time, with which to achieve the desired transfer. This is done by "stacking" additional revolutions of the staging orbit prior to departure on the unstable manifold path.[25] Four additional revolutions on the staging orbit are added to the initial guess displayed in Figure 14(a). Thus, the initial guess passed to COLT consists of these four revolutions, the unstable manifold trajectory, and the values of τ_{spiral}, ν_{SOI}, and m_{SOI} that produce the low-thrust spiral displayed in 14(a). With this initial guess COLT computes the low-thrust transfer in Figure 14(b), which requires approximately 228 days and 0.52 kg of propellant to achieve. The solution displayed in Figure 14(b) shows that the stacked staging orbit revolutions included in the initial guess are distributed by the direct collocation algorithm into a quasi-periodic-like structure. This new motion is even more evident in Figure 15(a), a three-dimensional view of the transfer. After moving along this structure the spacecraft departs the vicinity of the staging orbit and conducts a powered lunar flyby to insert on the explicitly propagated low-thrust spiral trajectory. This geometry is influenced by the initial guess which also includes an unstable manifold trajectory with a close lunar flyby.

Several important differences exist between the convergence process for Phase 1 and 2 transfers. First, the initial mass used to converge a Phase 2 transfer must be the final mass of a converged Phase 1 transfer. In this case, the final mass of the transfer shown in Figure 11 is used as the initial mass for the transfer in Figure 14(b). The spacecraft mass is the only parameter from Phase 1 that must be carried over to compute Phase 2. Furthermore, the spacecraft mass and the maximum thrust, T_{max}, determine the maximum acceleration that the spacecraft can produce. When convergence difficulty is encountered it is frequently advantageous to temporarily raise the maximum available acceleration by first computing a transfer that uses a T_{max} value slightly higher than that available to LIC. Then, a natural parameter continuation process can be used to lower T_{max} to the correct value. Continuation is employed to obtain both staging to science orbit transfers presented in this investigation. Finally, as stated previously, because the low-thrust spiral phase of the staging to science orbit transfer is explicitly propagated with a sub-optimal control law the resulting transfer is not fully optimal. Instead the objective of the direct collocation problem in this phase is to maximize the mass at the connection point between the trajectory computed with collocation and the explicitly propagated low-thrust spiral.

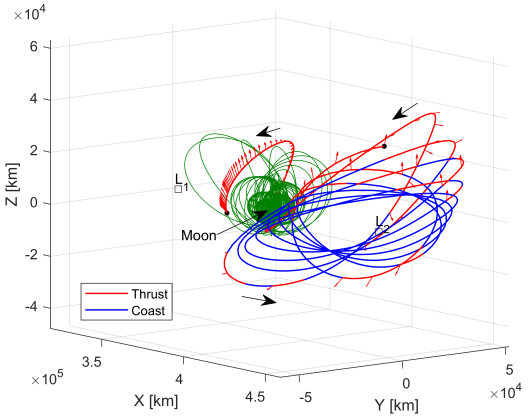

(a) Near Moon Transfer

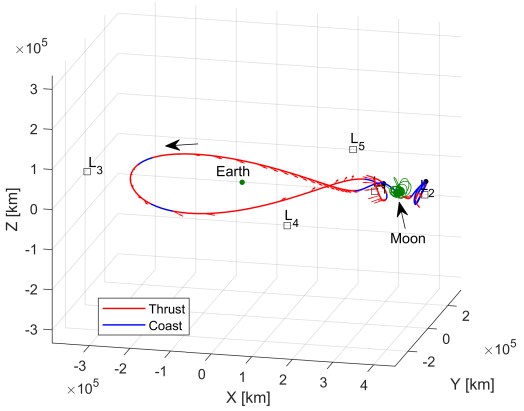

(b) Around Earth Transfer

Fig. 15: Out-of-plane views of two different transfers for Phase 2 plotted in the Earth-Moon rotating frame.

Phase 2 transfers generally fall into one of two categories: transfers that remain near the Moon, as seen already, and those that include at least one loop around the Earth. The latter of these two options is examined by generating a new Phase 2 map. A close connection is identified on a Phase 2 map generated with events at a Sun angle of 315°, and the resulting initial guess is displayed in Figure 16(a). In this case, the difference in position between the end of the unstable manifold trajectory and the beginning of the low-thrust spiral is especially large. However, these two points are relatively close in energy and in velocity direction. Thus, the NN search algorithm identifies this initial guess that may have

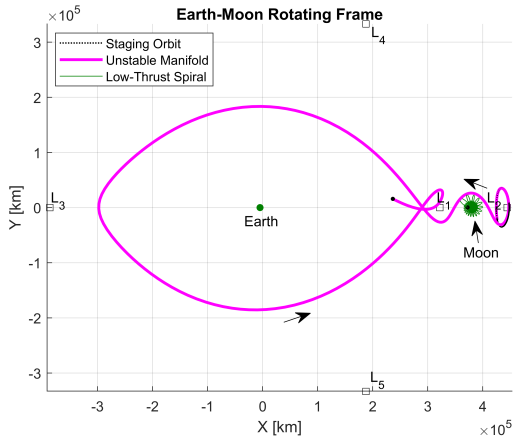

(a) Initial Guess

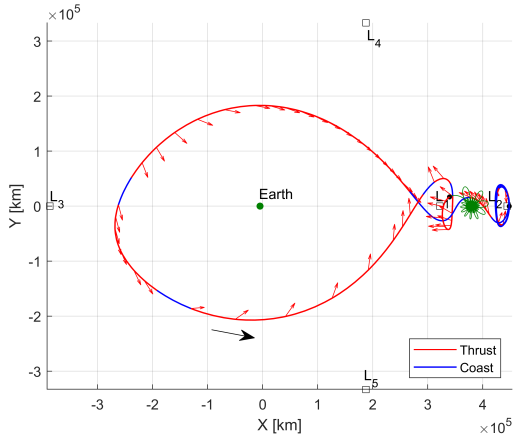

(b) Converged Result

Fig. 16: Initial guess and direct collocation result for Phase 2 transfer in the Earth-Moon rotating frame that includes a loop around the Earth. This transfer takes 212 days and consumes 0.52 kg of propellant.

been disregarded by a visual inspection. Despite the seemingly large discontinuity, COLT uses this initial guess to compute the low-thrust transfer shown in Figure 16(b). This transfer delivers the spacecraft from the staging orbit to the science orbit in 212 days and requires roughly the same propellant mass as the previous case, 0.52 kg. Figures 16(b) and 15(b) illustrate that rather than using repeated revolutions near the staging orbit, most of the plane change required to begin the spiral down to the science orbit is completed during the transit around the Earth. This behavior, and the lack of a low-altitude Lunar flyby, make this transfer and others like it easier to converge because the larger distance from the Moon decreases the sensitivity of the optimization problem.

Combining the results computed for phases 1 and 2 of the LIC trajectory yields complete deployment to science orbit trajectories. The sample LIC trajectories computed in the BCR4BP using the proposed framework are summarized in Table 3. The Phase 1 transfer without an Earth flyby, shown in Figure 11, is labeled A while the transfer that includes the Earth flyby, displayed in Figure 13, is B. Similarly, the Phase 2 transfer that remains near the Moon, depicted in Figure 14(b), is labeled C and the transfer that loops around the Earth, shown in Figure 16(b), is D. Note that for all transfer combinations up to a month of additional transfer time may be added to account for the phasing time that must be included in the staging orbit following Phase 1 of the transfer. This time allows the spacecraft to reach the state and Sun angle required to begin Phase 2. In this case, the maximum phasing time required is 25 days and the minimum is 0.5 days. The transfer times and propellant consumption values provided in Table 3 are comparable to the current baseline trajectory shown in Figure 1 which requires 318 days and 0.69 kg of propellant.

The transfers computed with the demonstrated framework all require more time and propellant than the baseline transfer, however, several steps are available to reduce the time and change in mass of the transfers in Table 3. First, refinement of the maps and NN search algorithm used to compute a Phase 2 transfer could reduce the time of flight and propellant mass required for this phase where these quantities are the largest. Alternate maps or search criteria for the NN algorithm could generate initial guesses that lead to improved transfer performance. Second, while the additional staging orbit revolutions added to the initial guess for the staging to science orbit phase are useful for achieving convergence it may be possible to remove some of them after a transfer is converged. For example, some of the revolutions near the staging orbit that appear in Figure 15(a) could likely be removed because they consist largely of long coast segments. If possible, removing excess trajectory will reduce transfer time. Another step for improving the transfers is using a multi-phase collocation algorithm to solve the staging to science orbit phase. A multi-phase approach would permit the low-thrust spiral to the science orbit to be fully optimized, thereby increasing the spacecraft mass at SOI. The majority of propellant consumption occurs during the low-thrust spiral, thus optimizing this section of trajectory could

offer significant propellant savings. These three steps can lead to reductions in both time of flight and propellant consumption for the LIC transfer.

Table 3: Summary of sample transfers. All results are from the given deployment state to the science orbit. Given characteristics are time of flight (TOF), final mass (m_f), and total change in mass (Δm).

Transfer	TOF [days]	m_f [kg]	Δm [kg]
A $\rightarrow$ C	369.25	13.25	0.75
B $\rightarrow$ C	371.88	13.24	0.76
A $\rightarrow$ D	353.02	13.24	0.76
B $\rightarrow$ D	382.34	12.87	1.13
Baseline	318	13.31	0.69

5. Concluding Remarks

The proposed framework for constructing a LIC baseline trajectory addresses the need for a design methodology that is both robust and flexible. Employing a dynamical model that includes the Sun enables the perturbing acceleration of this body to be leveraged to achieve the desired transfer despite LIC's limited control authority. Moreover, utilizing direct collocation to converge initial guesses developed in the BCR4BP allows a wider range of guesses to be used due to the robustness of this algorithm. Flexibility is further enhanced by using a staging orbit to separate the LIC trajectory into two halves that can be designed independently. Together these design choices offer a framework to systematically generate a variety of transfer configurations with time of flight and propellant consumption values comparable to the current baseline. Further improvements to this procedure could increase the efficiency of the process, enhance the quality of the solutions it generates, and broaden its applicability to missions beyond LIC.

Several steps for improving the design methodology are immediately evident. First, other staging orbits should be examined, particularly quasi-periodic orbits (QPOs). In the BCR4BP, QPOs are especially useful because they do not require a resonance with the synodic period of the Sun; thus, there is a larger number of options available for use as a staging orbit. Furthermore, the Phase 2 transfer shown in Figure 15(a) appears to leverage quasi-periodic structures indicating that this type of orbit may be preferable for use as a staging orbit. Another potential improvement to the design methodology is increased insight for selecting a Sun angle that locates the hyperplanes for the Phase 1 and 2 maps. Currently, a trial and error process is used to to identify Sun angles that generate maps which contain events with close matches. However, there is likely a more informed approach that can be taken for this step of the design process. Refining this step, along with making improvements to how the NN search algorithm is used to identify close matches between events, may alleviate some of the convergence challenges encountered in Phase 2. Finally, the results computed in this investigation should be validated in a full ephemeris model to confirm their applicability to flight operations. All of these enhancements would increase the usefulness of the proposed framework; however, even in the present state this strategy offers a powerful approach for designing low-thrust trajectories for a cislunar CubeSat.

Acknowledgements

The authors thank the Purdue University School of Aeronautics and Astronautics for facilities and support, including access to the Rune and Barbara Eliasen Visualization Laboratory. Additionally, many thanks to the members of the Purdue Multi-Body Dynamics Research Group for interesting discussions and ideas. Special thank you to Nicholas LaFarge for the idea of employing a nearest neighbor search algorithm and for guidance on its implementation. This research is supported by NASA Space Technology Research Fellowship, NASA Grant NNX16AM42H. Some analysis was conducted at the NASA Goddard Space Flight Center.

References

[1] J. Schoolcraft, A. T. Klesh, and T. Werne. MarCO: Interplanetary Mission Development On a CubeSat Scale. In *SpaceOps 2016 Conference*, SpaceOps Conferences. American Institute of Aeronautics and Astronautics, May 2016.

[2] P. Clark, B. Malphrus, R. MacDowall, D. C. Folta, A. Mandell, C. Brambora, D. Patel, S. Banks, K. Hohman, V. Hruby, K. Brown, J. Kruth, and R. Cox. Lunar Ice Cube: Determining Volatile Systematics Via Lunar Orbiting Cubesat. *European Planetary Science Congress*, 10:EPSC2015–61, Oct 2015.

[3] A. J. Mazarr and D. C. Folta. Low-Thrust Station-Keeping for a Highly Elliptical Polar Orbit at the Moon. In *AAS/AIAA Astrodynam-*

ics Specialist Conference, pages 1–31, Snowbird, Utah, 2018.

[4] Busek Space Propulsion and Systems.

[5] M. D. Rayman, P. Varghese, D. H. Lehman, and L. L. Livesay. Results from the Deep Space 1 Technology Validation Mission. *Acta Astronautica*, 47(2-9):475–487, 2000.

[6] C. Russell and C. Raymond, editors. *The Dawn Mission to Minor Planets 4 Vesta and 1 Ceres*. Springer-Verlag, New York, 1 edition, 2012. ISBN 978-1-4614-4902-7.

[7] R. Mathur. Low Thrust Trajectory Design and Optimization: Case Study of a Lunar CubeSat Mission. In *6th International Conference on Astrodynamics Tools and Techniques*, pages 1–11, Darmstadt, Germany, 2016. Emergent Space Technologies, Inc.

[8] N. Bosanac. *Leveraging Natural Dynamical Structures to Explore Multi-Body Systems*. Ph.D. Dissertation, Purdue University, 2016.

[9] N. Bosanac, A. D. Cox, K. C. Howell, and D. C. Folta. Trajectory design for a cislunar cubesat leveraging dynamical systems techniques: The lunar icecube mission. In *27th AAS/AIAA Space Flight Mechanics Meeting*, San Antonio, Texas, February 2017.

[10] N. Bosanac, A. D. Cox, K. C. Howell, and D. C. Folta. Trajectory design for a cislunar CubeSat leveraging dynamical systems techniques: The Lunar IceCube mission. *Acta Astronautica*, 144: 283–296, 2018.

[11] D. C. Folta, N. Bosanac, A. D. Cox, and K. C. Howell. The lunar icecube mission design: Construction of feasible transfer trajectories with a constrained departure. *Advances in the Astronautical Sciences*, 158:1369–1387, 2016.

[12] W. S. Koon, M. W. Lo, J. E. Marsden, and S. D. Ross. Low energy transfer to the moon. *Celestial Mechanics and Dynamical Astronomy*, 81(1):63–73, 2001.

[13] G. Gómez, W. Koon, M. Lo, J. Marsden, J. Masdemont, and S. Ross. Invariant manifolds, the spatial three-body problem and space mission design. *Advances in the Astronautical Sciences*, 109:3–22, 2002.

[14] J. Parker and M. Lo. Shoot the moon 3d. *Advances in the Astronautical Sciences*, 123:2067–2086, 2006.

[15] G. Mingotti, F. Topputo, and F. Bernelli-Zazzera. Low-energy, low-thrust transfers to the Moon. *Celestial Mechanics and Dynamical Astronomy*, 105(1):61–74, 2009.

[16] A. Zanzottera, G. Mingotti, R. Castelli, and M. Dellnitz. Intersecting invariant manifolds in spatial restricted three-body problems: Design and optimization of Earth-to-halo transfers in the Sun-Earth-Moon scenario. *Communications in Nonlinear Science and Numerical Simulation*, 17(2):832–843, 2012.

[17] P. J. Enright and B. A. Conway. Discrete Approximations to Optimal Trajectories Using Direct Transcription and Nonlinear Programming. *Journal of Guidance, Control, and Dynamics*, 15 (4):994–1002, 1992.

[18] D. J. Grebow, M. T. Ozimek, and K. C. Howell. Design of Optimal Low-Thrust Lunar Pole-Sitter Missions. *The Journal of Astronautical Sciences*, 58(1):55–79, 2011.

[19] R. L. Parker Jeffrey S.; Anderson. *Low-Energy Lunar Trajectory Design*. Deep Space Communications and Navigation Systems, Jet Propulsion Laboratory, Pasadena, California, 2013.

[20] G. Mingotti, F. Topputo, and F. Bernelli-Zazzera. Efficient invariant-manifold, low-thrust planar trajectories to the Moon. *Communications in Nonlinear Science and Numerical Simulation*, 17(2):817–831, 2012.

[21] Y. Cheng, G. Gómez, J. J. Masdemont, and J. Yuan. Study of the transfer between libration point orbits and lunar orbits in EarthMoon system. *Celestial Mechanics and Dynamical Astronomy*, 128(4):409–433, 2017.

[22] P. Cao, B. He, and H. Li. Analysis of direct transfer trajectories from LL2 halo orbits to LLOs. *Astrophysics and Space Science*, 362 (9), 2017.

[23] K. K. Boudad. Disposal Dynamics From The Vicinity Of Near Rectilinear Halo Orbits In The Earth-Moon-Sun System. Master's Thesis, Purdue University, 2018.

[24] N. L. Parrish, J. S. Parker, S. P. Hughes, and J. Heiligers. Low-Thrust Transfers From Distant Retrograde Orbits To L2 Halo Orbits in the Earth-Moon System. In *International Conference on Astrodynamics Tools and Techniques*, Darmstadt, Germany, 2016.

[25] R. E. Pritchett, E. Zimovan, and K. C. Howell. Impulsive and Low-Thrust Transfer Design Between Stable and Nearly-Stable Periodic Orbits in the Restricted Problem. In *2018 AIAA/AAS Space Flight Mechanics Meeting*, Orlando, Florida, 2018. ISBN 978-1-62410-533-3.

[26] D. J. Grebow and T. A. Pavlak. MColl:

Monte Collocation Trajectory Design Tool. In *AAS/AIAA Astrodynamics Specialist Conference*, Stevenson, Washington, 2017.

[27] R. E. Pritchett. Numerical Methods for Low-Thrust Trajectory Optimization. Master's Thesis, Purdue University, 2016.

[28] A. Wachter and L. T. Biegler. On the Implementation of a Primal-Dual Interior Point Filter Line Search Algorithm for Large-Scale Nonlinear Programming. *Mathematical Programming*, 106 (1):25–57, 2006.

[29] G. Shakhnarovich, P. Indyk, and T. Darrell. Introduction. In *Nearest-Neighbor Methods in Learning and Vision*, chapter 1, pages 1–12. MIT Press, Cambridge, Massachusetts, 1 edition, 2005.

[30] K. L. Clarkson. Nearest-Neighbor Searching and Metric Space Dimensions. In *Nearest-Neighbor Methods in Learning and Vision*, chapter 2, pages 15–59. MIT Press, Cambridge, Massachusetts, 1 edition, 2005.

[31] M. Vaquero and J. Senent. Poincare : A Multi-Body, Multi-System Trajectory Design Tool. In *7th International Conference on Astrodynamics Tools and Techniques*, pages 1–12, Oberpfaffenhofen, Germany, 2018.

[32] R. D. Falck, N. Glenn, and J. W. Dankanich. Optimization of Low-Thrust Spiral Trajectories by Collocation. In *AIAA/AAS Astrodynamics Specialist Conference*, number August, pages 1–17, Minneapolis, Minnesota, 2012. ISBN 2012217699.

[33] Z. P. Olikara. Framework for Optimizing Many-Revolution Low-Thrust Transfers. In *AAS Astrodynamics Specialists Conference*, pages 1–19, Snowbird, Utah, 2018.